Noninvasive O_6 Methylguanine-DNA Methyltransferase Status Prediction in Glioblastoma Multiforme Cancer Using Magnetic Resonance Imaging Radiomics Features: Univariate and Multivariate Radiogenomics Analysis

Ghasem Hajianfar[1,2], Isaac Shiri[3], Hassan Maleki[2], Niki Oveisi[4], Abbas Haghparast[1], Hamid Abdollahi[6], Mehrdad Oveisi[2,5]

BACKGROUND: **This study aimed to predict methylation status of the O_6 methylguanine-DNA methyltransferase (MGMT) gene promoter status by using magnetic resonance imaging radiomics features, as well as univariate and multivariate analysis.**

METHODS: **Eighty-two patients who had an MGMT methylation status were included in this study. Tumors were manually segmented in the 4 regions of magnetic resonance images, 1) whole tumor, 2) active/enhanced region, 3) necrotic regions, and 4) edema regions. About 7000 radiomics features were extracted for each patient. Feature selection and classifier were used to predict MGMT status through different machine learning algorithms. The area under the curve (AUC) of the receiver operating characteristic curve was used for model evaluations.**

RESULTS: **Regarding univariate analysis, the Inverse Variance feature From Gray Level Co-occurrence Matrix in whole tumor segment with 4.5 mm Sigma of Laplacian of Gaussian filter with AUC of 0.71 (P value = 0.002) was found to be the best predictor. For multivariate analysis, the Decision Tree classifier with Select from Model feature selector and LOG (Laplacian of Gaussian) filter in edema region had the highest performance (AUC, 0.78), followed by Ada-Boost classifier with Select from Model feature selector and LOG filter in edema region (AUC, 0.74).**

CONCLUSIONS: **This study showed that radiomics using machine learning algorithms is a feasible noninvasive approach to predict MGMT methylation status in patients with glioblastoma multiforme cancer.**

INTRODUCTION

Glioblastoma multiforme (GBM) is one of the most aggressive malignant brain tumors, with an occurrence of 2–3 cases per 100,000 individuals.[1] After diagnosis, these patients have a median survival of 15 months, with <5% of patients having a 5-year survival.[2] This poor prognosis results from the intratumor genetic heterogeneous pattern of GBM.[3]

Temozolomide (TMZ) is at the forefront in therapy for patients with GBM. This treatment causes alkylation at the O_6 guanine of DNA, subsequently inducing cytotoxic effects and death in cancer cells.[4] Studies show that the methylation status of the O_6 methylguanine-DNA methyltransferase (MGMT) gene promoter could be a predictor for the efficacy of TMZ treatment.[5] MGMT is a

Key words
- GBM
- MGMT
- MRI
- Radiomics
- Radiogenomics

Abbreviations and Acronyms
AB: Ada-Boost
AUC: Area under the curve
CE: Contrast-enhanced
FLAIR: Fluid-attenuated inversion recovery
GBM: Glioblastoma multiforme
GLCM: Gray Level Co-occurrence Matrix
LOG: Laplacian of Gaussian
MGMT: O_6 methylguanine-DNA methyltransferase
MRI: Magnetic resonance imaging
ROC: Receiver operating characteristic
T1-W: T1-weighted
T2-W: T2-weighted
TMZ: Temozolomide
WT: Whole Tumor

From the [1]Department of Medical Physics, Faculty of Medicine, Kermanshah University of Medical Sciences, Kermanshah, Iran; [2]Rajaie Cardiovascular Medical and Research Center, Iran University of Medical Science, Tehran, Iran; [3]Division of Nuclear Medicine and Molecular Imaging, Department of Medical Imaging, Geneva University Hospital, Geneva, Switzerland [4]School of Population and Public Health and [5]Department of Computer Science, University of British Columbia, Vancouver, BC, Canada; and [6]Department of Radiologic Sciences and Medical Physics, Faculty of Allied Medicine, Kerman University of Medical Sciences, Kerman, Iran

Citation: World Neurosurg. (2019) 132:e140-e161.
https://doi.org/10.1016/j.wneu.2019.08.232

*Journal homepage: **www.journals.elsevier.com/world-neurosurgery***

*Available online: **www.sciencedirect.com***

vital gene, which encodes a DNA repair protein. Tumor cells with MGMT expression show resistance to TMZ, whereas tumor cells without MGMT expression are more sensitive to TMZ. Demethylation of the DNA O-6 guanine by MGMT prohibits the DNA degradation induced by TMZ. Patients with GBM with MGMT promoter silencing show a higher response to TMZ. Several studies have shown that MGMT promoter methylation is associated with longer survival.[6-8]

In patients with GBM without surgical resection indications, it has been shown that medical imaging could help understand the tumor pathology.[9] Clinical studies have indicated that magnetic resonance imaging (MRI) sequences such as T1-weighted (T1-W), T1-contrast, T2-weighted (T2-W), and fluid-attenuated inversion recovery (FLAIR) have a feasible role for the prognosis, diagnosis, and treatment plan for GBM.[10] In addition, further research studies have introduced radiomics as a novel field that can also be used as a powerful prognostic tool.[11-13] In combination with MRI sequences, these tools can have a major impact on management of patients with GBM through higher stratification.[14]

Radiomics is an advanced image processing technique that extracts many quantitative features with standard and special algorithms. These features are then correlated with clinical outcomes. The features are shape, intensity, and texture based. The features are used during clinical decision making for patient diagnosis, prognosis, and therapy response prediction/assessment.[15-17] An extension of this field is radiogenomics, in which radiomics features are correlated with genomics parameters.[18]

Tissue sampling with surgical resection is the gold standard for the determination of MGMT promoter methylation status. However, this method has limitations, such as GBM heterogeneity, a large volume of tissue specimens, and the cost of testing in clinics in which it is not routine.[19,20] Recently, radiomics features have been used as imaging biomarkers in MGMT methylation status prediction.[21,22] These quantitative features are reported to simplify the optimum tissue specimen at surgery.[23] Multiple studies have explored the efficacy of using these quantitative features in MGMT methylation status prediction. A study by Iliadis et al.[24] showed that necrosis volume is inversely associated with MGMT protein−positive tumor cells. Furthermore, a study by Levner et al. used neural networks as a classifier with S-transform texture features acquired from MRI sequences (T2-W, FLAIR, and T1-W contrast-enhanced [CE]) and achieved >87% accuracy for the prediction of MGMT methylation status.[25] In addition, a study by Eoli et al. reported that CE regions of tumors are correlated with an unmethylated status.[26] Moreover, a study by Drabycz et al.[27] evaluated VASARI (Visually Accessible Rembrandt Images) and automatic texture features for the prediction of MGMT methylation status. The results showed that incorporating VASARI with texture features improves the predictive power of

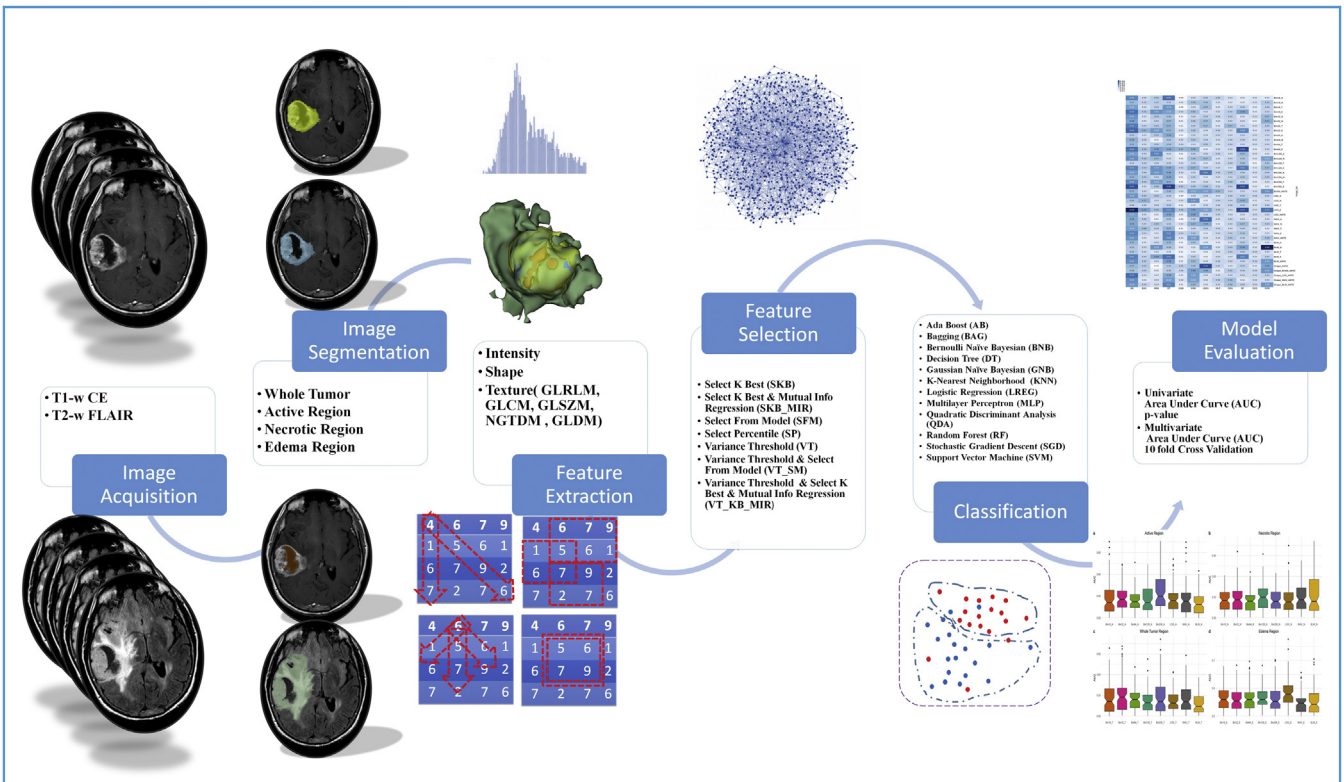

Figure 1. The process flow followed in the study. AUC, are under the curve; CE, contrast-enhanced; FLAIR, fluid-attenuated inversion recovery; GLCM, Gray Level Co-Occurrence Matrix; GLDM, Gray Level Dependence Matrix; GLRLM, Gray Level Run Length Matrix; GLSZM, Gray Level Size Zone Matrix; NGTDM, Neighboring Gray Tone Difference Matrix; T1-w, T1-weighted; T2-w, T2-weighted.

Table 1. Clinical Characteristics of MGMT Status Data Set

Characteristic	Value (Number of Patients = 82)
Gender	
Male	46 (56.1)
Female	36 (43.9)
Age (years)	57.4 ± 13.9
MGMT status	
Methylation	45 (54.9)
Unmethylation	37 (45.1)
Karnofsky Performance Status	
<70	51 (62.2)
>70	23 (28)
Not available	8 (9.8)

Values are number (%) except where indicated otherwise.

MGMT methylation status. In another study, Moon et al.[21] found that there are several correlations between MGMT methylation status and features extracted from computed tomography and T2* dynamic susceptibility CE perfusion-weighted imaging and diffusion tensor imaging MRI features.

This study aims to predict MGMT status by using T2-W and T1-W MRI radiomics features, along with univariate and multivariate analysis.

Table 2. Feature selection and Classification methods

	Feature Selection Methods	Abbreviation
1	Select K best	KB
2	Select K best and mutual info regression	KB-MIR
3	Select from model	SM
4	Select percentile	SP
5	Variance threshold	VT
6	Variance threshold and select from model	VT-SM
7	Variance threshold and select K best and mutual info regression	VT-KB-MIR

	Classification Methods	Abbreviation
1	Adaptive boost	AB
2	Bagging	BAG
3	Naive Bayes	NB
4	Decision tree	DT
5	Gaussian naive Bayes	GNB
6	K-nearest neighbors	KNN
7	Logistic regression	LREG
8	Multilayer perceptron	MLP
9	Quadratic discriminant analysis	QDA
10	Random forest	RF
11	Stochastic gradient descent	SGD
12	Support vector machine	SVM

METHODS

Figure 1 shows the process flow followed in this study.

GBM Patient Data Set

In this study, 122 patients with pathologically confirmed GBM who had 2 MRI sequences (T2 FLAIR and T1-W CE) were included. All images were downloaded from The Cancer Imaging Archive.[28,29] Clinical data from The Cancer Genome Atlas[30] and Bady et al.[31] were used to determine the MGMT methylation status using probe cg12434587 and cg12981137 values on HumanMethylation27 and HumanMethylation450 databases. A total of 82 patients who had an MGMT methylation status were kept in this study, whereas the remainder of the data were excluded. Table 1 outlines the clinical characteristics of the patients included in this study.

Segmentation

Tumors were manually segmented with a three-dimensional slicer in the following 4 regions 1) whole tumor (WT), 2) active/enhanced tumor (A), 3) necrotic regions (N) in T1-W CE, and 4) edema regions (E) in T2 FLAIR imaging. All segmentations were verified by an expert radiologist.

Feature Extraction

Before feature extraction, the images were preprocessed. For preprocessing, images were discretized and resampled to 16, 32, 64, 128, 2, and 56 Gy level bin sizes. In addition, wavelet with different decompositions (HHH, HHL, HLH, HLL, LHH, LHL, LLH, and LLL) and Laplacian of Gaussian (LOG) filters with different sigma values (0.5–5 with step 0.5) were applied. Feature extraction included 3 feature sets: shape based, first order, and textures. Thirteen shape features were extracted for each segment along with A/WT ratios, N/WT ratios, and WT/E ratios for the features. Texture sets were Gray Level Co-occurrence Matrix (GLCM), Gray Level Run Length Matrix, Gray Level Dependence Matrix, Gray Level Size Zone Matrix, and Neighboring Gray Tone Difference Matrix (Supplementary Table 1). About 8519 features were extracted for each patient, and 41 image sets were prepared for model evaluations (Supplementary Table 2).

Feature Selection

Seven different feature selections methods were used in the framework and performances were compared (Table 2).

Classifiers

Twelve Classifiers were implemented and compared (Table 2). The details of each classifier are provided in Supplementary Table 3.

Evaluation

For univariate analysis, each feature value was normalized to obtain Z scores, followed by Student t test for comparison. A P

Table 3. Top Univariate Analysis Sorted by Area Under the Curve

Features	Filter	Region	Area Under the Curve	*P* Value
GLCM_IV	LOG_4.5S	Whole tumor	0.71	0.003
GLCM_IV	LOG_5.0S	Whole tumor	0.70	0.003
GLCM_IV	LOG_4.0S	Whole tumor	0.69	0.008
NGTDM_Strength	LOG_2.0S	Whole tumor	0.68	0.050
GLCM_IV	LOG_4.5S	Active	0.68	0.024
FO_Skewness	LOG_4.5S	Edema	0.68	0.010
GLCM_IV	LOG_5.0S	Active	0.68	0.014
GLDM_DV	W_LLL	Necrosis	0.68	0.050
GLSZM_LALGLE	LOG_5.0S	Necrosis	0.68	0.063
NGTDM_Strength	LOG_5.0S	Necrosis	0.68	0.410
GLCM_IV	W_LLL	Necrosis	0.68	0.004
GLDM_LDE	W_LLL	Necrosis	0.67	0.022
GLCM_IDM	W_LLL	Necrosis	0.67	0.010
FO_Kurtosis	LOG_2.5S	Edema	0.67	0.002
NGTDM_Complexity	W_LLL	Necrosis	0.67	0.213
GLCM_Id	W_LLL	Necrosis	0.67	0.012
NGTDM_Strength	LOG_2.0S	Necrosis	0.67	0.055
NGTDM_Strength	LOG_2.5S	Necrosis	0.67	0.273
NGTDM_Complexity	LOG_2.0S	Whole tumor	0.67	0.148
FO_Kurtosis	LOG_2.0S	Edema	0.67	0.007

GLCM, Gray Level Co-occurrence Matrix; NGTDM, Neighboring Gray Tone Difference Matrix; FO, first order; GLDM, Gray Level Dependence Matrix; GLSZM, Gray Level Size Zone Matrix.

value of <0.05 was used as a criterion for statistically significant results. Area under the curve (AUC) of the receiver operating characteristic curve was used to determine which feature could predict MGMT methylation status. Statistical analysis for this portion was performed in R 3.5.1 (using 'pROC' and 'stats' packages [R Foundation for Statistical Computing, Vienna, Austria]).

For multivariate analysis, an in-house developed python framework was used. A 10-fold cross-validation was applied for model evaluation. Furthermore, the AUC of receiver operating characteristic curves was also used for model evaluations. Heatmaps and boxplots were constructed to compare different developed models. The cross-combinations of feature selections and classification methods were shown as a heat map (using mean AUC values in cross-validation).

RESULTS

Table 3 summarizes univariate analyses sorted according to AUC values in the top 20 features with different filters and segments. The best predictor of MGMT methylation status was the Inverse Variance feature of GLCM (GLCM_IV) in a WT segment with 4.5 mm Sigma of LOG filter (LOG_4.5S) (AUC, 0.71; $P = 0.002$). Table 4 summarizes the univariate analyses of shape features. Sphericity in the Active region (AUC, 0.62; $P = 0.06$) and elongation and flatness in Edema regions (AUC, 0.62; $P = 0.08$) had better performances in the prediction of MGMT methylation status.

The Decision Tree classifier with Select from Model feature selector (DT_SFM) in LOG filter in edema region (E) features had the highest performance (AUC, 0.78). The Ada-Boost (AB) classifier with Select from Model feature selector in LOG filter (AB_SFM) in edema regions (E) features (AUC, 0.74) follows in highest performance (Supplementary Figure 4).

Figure 2 summarizes the results regarding MGMT mutation status prediction based on feature selection and image sets. According to these results, the feature selection performance had a range of 0.52–0.61. In addition, a combination of the Select from Model feature selector (SFM) + the LOG filter in Edema region (E) had the highest performance (AUC, 0.61), followed by a combination of the Variance Threshold and the Select from Model feature selector (VT_SFM) + LOG filter in Edema region (E) (AUC, 0.6).

Figure 3 shows the results regarding MGMT mutation status prediction based on feature classification and image sets. According to these results, classification performance had a range of 0.50–0.68. Support Vector Machine classifier (SVM) + combination of Bin 64, LOG, and Wavelet (BLW)

Table 4. Univariate Analysis of Shape Features

	Active		Necrosis		Whole Tumor		Edema	
Features	**AUC**	***P* Value**	**AUC**	***P* Value**	**AUC**	***P* Value**	**AUC**	***P* Value**
Elongation	0.58	0.19	0.58	0.15	0.55	0.43	0.62	0.08
Flatness	0.51	0.51	0.53	0.50	0.51	0.82	0.62	0.08
Least axis	0.51	0.78	0.53	0.35	0.54	0.66	0.53	0.60
Minor axis	0.52	0.66	0.54	0.21	0.53	0.55	0.53	0.96
Major axis	0.52	0.60	0.51	0.92	0.51	0.88	0.55	0.31
Maximum 2D diameter column	0.52	0.52	0.54	0.22	0.55	0.36	0.51	0.63
Maximum 2D diameter row	0.50	0.82	0.50	0.89	0.51	0.92	0.56	0.38
Maximum 2D diameter slice	0.52	0.47	0.50	0.89	0.54	0.38	0.55	0.43
Maximum 3D diameter	0.51	0.87	0.52	0.81	0.56	0.19	0.54	0.50
Sphericity	0.62	0.06	0.55	0.33	0.55	0.43	0.54	0.64
Surface area	0.52	0.63	0.54	0.29	0.52	0.73	0.51	0.75
Surface volume ratio	0.58	0.20	0.52	0.98	0.51	0.52	0.54	0.55
Volume	0.52	0.45	0.54	0.60	0.50	0.83	0.53	0.58
A/T volume ratio	0.54	0.48						
N/T volume ratio	0.56	0.57						
T/E volume ratio	0.52	0.76						

filters in Necrosis region (N) had the highest performance (AUC, 0.68). This finding is followed by Ada-Boost classifier (AB) + Bin 16 in Active region (A) (AUC, 0.68), Decision Tree classifier (DT) + Bin 256 in Edema region (E) (AUC, 0.66), and Random Forest classifier (RF) + Bin 256 Edema region (E) (AUC, 0.65).

Figure 4A and Supplementary Figure 1 (from the supplementary data) show the results for the prediction of MGMT mutation status in Active tumor regions. It is seen that model performance (mean AUC) had a wide range of 0.50–0.68 and Bin 256 had both the highest mean (AUC, 0.55) and the highest predictive performance (AUC, 0.68). Figure 4B and Supplementary Figure 2 (from the supplementary data) show the results for the prediction of MGMT mutation status in Necrosis tumor regions. Notable results include that model performance (mean AUC) had a wide range of 0.50–0.68, and a combination of Bin 64, LOG, and Wavelet filters (BLW) images had both the highest mean (AUC, 0.55) and the highest predictive performance (AUC, 0.68).

Figure 4C and Supplementary Figure 3 (from the supplementary data) show the results for the prediction of MGMT mutation status in WT regions. Model performance (mean AUC) had a wide range of 0.50–0.69, image set Bin 32 had the highest mean (AUC, 0.55), and image set Bin 256 had the highest predictive performance (AUC, 0.69). Figure 4D and Supplementary Figure 4 (from the supplementary data) show the results for the prediction of MGMT mutation status in Edema regions. It is seen that model performance (mean AUC) had a wide range of 0.50–0.78, and image set LOG filter had both the highest mean (AUC, 0.57) and the highest predictive performance (AUC, 0.78).

Figure 5A and Supplementary Figure 5 (from the supplementary data) show the results for the prediction of MGMT mutation status in a combination of all tumor regions. Results show that model performance (mean AUC) had a wide range of 0.50–0.68, image set Bin 64 had the highest mean (AUC, 0.56), and image set LOG filter and combination with shape features had the highest predictive performance (AUC, 0.68). Figure 5B shows the results regarding MGMT mutation status prediction based on feature selection. A combination of the Variance Threshold and the Select from Model feature selector (VT_SFM) had higher mean predictive performances than other feature selectors (AUC, 0.56). Figure 5A shows the results regarding MGMT mutation status prediction based on classifiers. The Ada-Boost classifier (AB) had a higher mean predictive performance than any other classifier (AUC, 0.59).

DISCUSSION

This study elaborated on an extensive radiomics technique that combines univariate and multivariate analysis with statistical and machine learning (ML) methods. This process was accomplished by using many features extracted from T1-W CE and T2-FLAIR images taken of 82 patients with GBM to predict their MGMT mutation status.

This study showed that GLCM_IV extracted from all segmented regions is an appropriate marker in predicting MGMT methylation status. Also, it was found that the Decision Tree classifier with Select from Model feature selector (DT_SFM) in LOG filter preprocessed in edema region (E) features had the highest

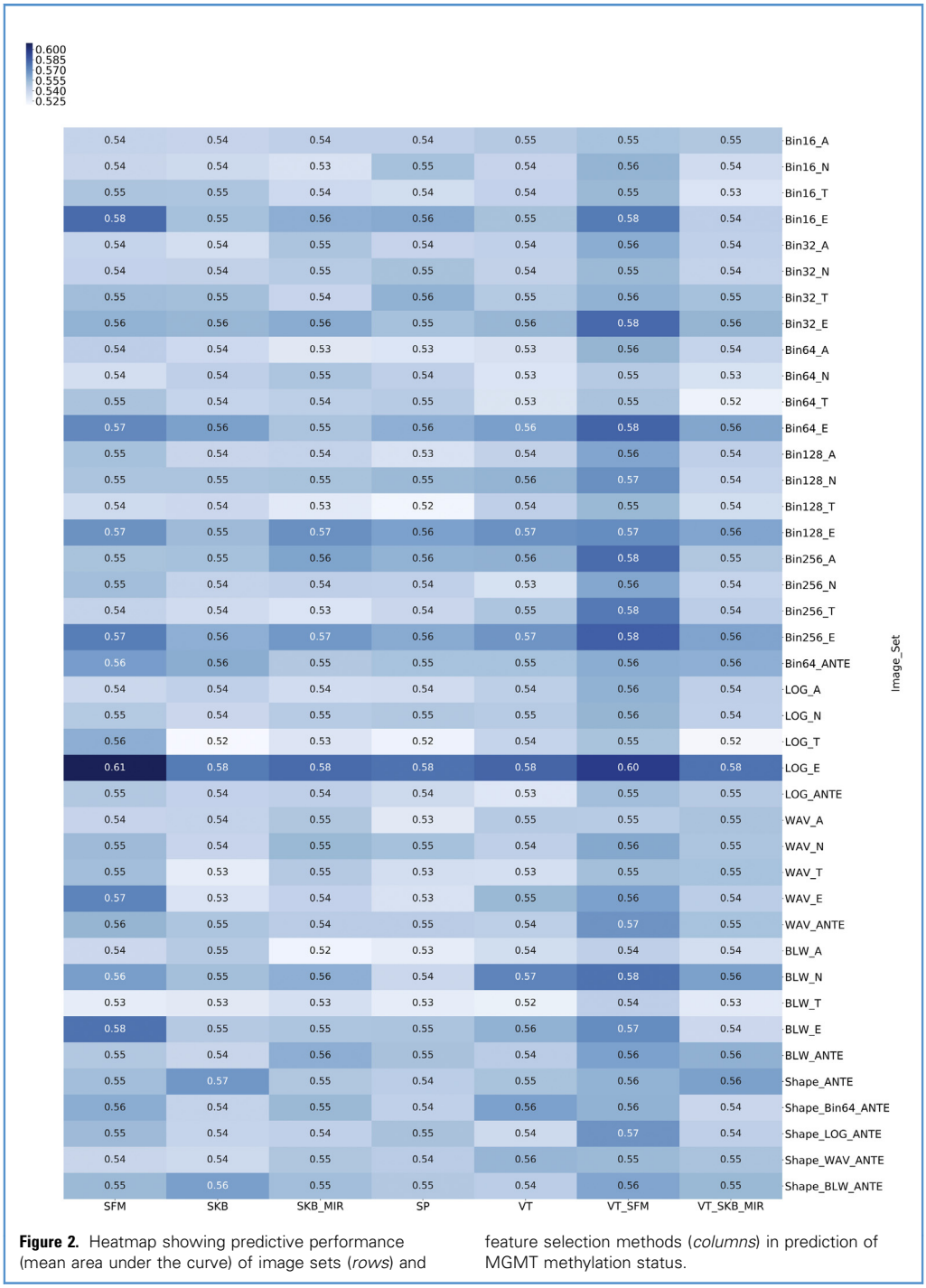

Figure 2. Heatmap showing predictive performance (mean area under the curve) of image sets (*rows*) and feature selection methods (*columns*) in prediction of MGMT methylation status.

performance (best model, AUC, 0.78). From the classifier and feature selections, AB and VT+SFM had higher mean performances, respectively. In the combinations of 4 segments among 8 image sets, Bin 64 had the highest mean and the LOG filter + shape features image set had the highest predictive performance (**Supplementary Figure 6** [from the **supplementary data**]).

Li et al.[32] tested the ability of univariate and multivariate analyses in the prediction of MGMT methylation status. Their study developed 2 multivariate radiomics models to predict MGMT methylation status in patients with GBM cancer. These investigators reported that there is a lack of a statistically significant difference in shape features between methylated and

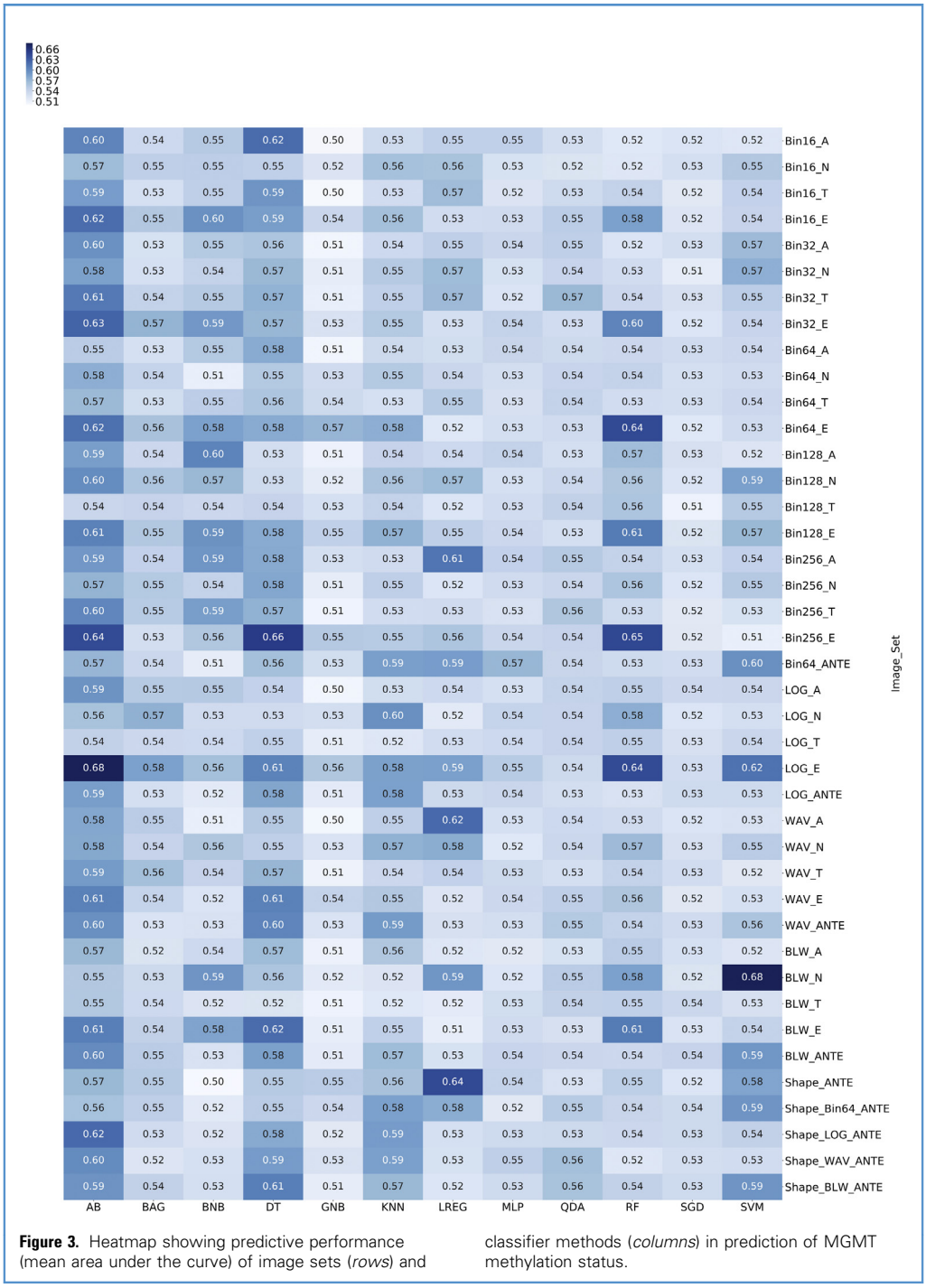

Figure 3. Heatmap showing predictive performance (mean area under the curve) of image sets (*rows*) and classifier methods (*columns*) in prediction of MGMT methylation status.

unmethylated MGMT tumors. Several studies have shown that there are no statistically significant differences in shape features between tumors with methylated versus unmethylated MGMT.[21,26,27,33,34] Similar to the current study, these studies found features that are correlated with parameters to MGMT methylation and could partake in model prediction. The results from the current study indicate that 3 shape features (sphericity in active region and elongation and flatness in edema region) have AUC >0.6 (see **Table 4**). In addition, **Figure 5A** shows that combination shape features with LOG filters could improve prediction.

Regarding classification algorithms used to predict MGMT methylation status, Korfiatis et al.[23] applied a Support Vector

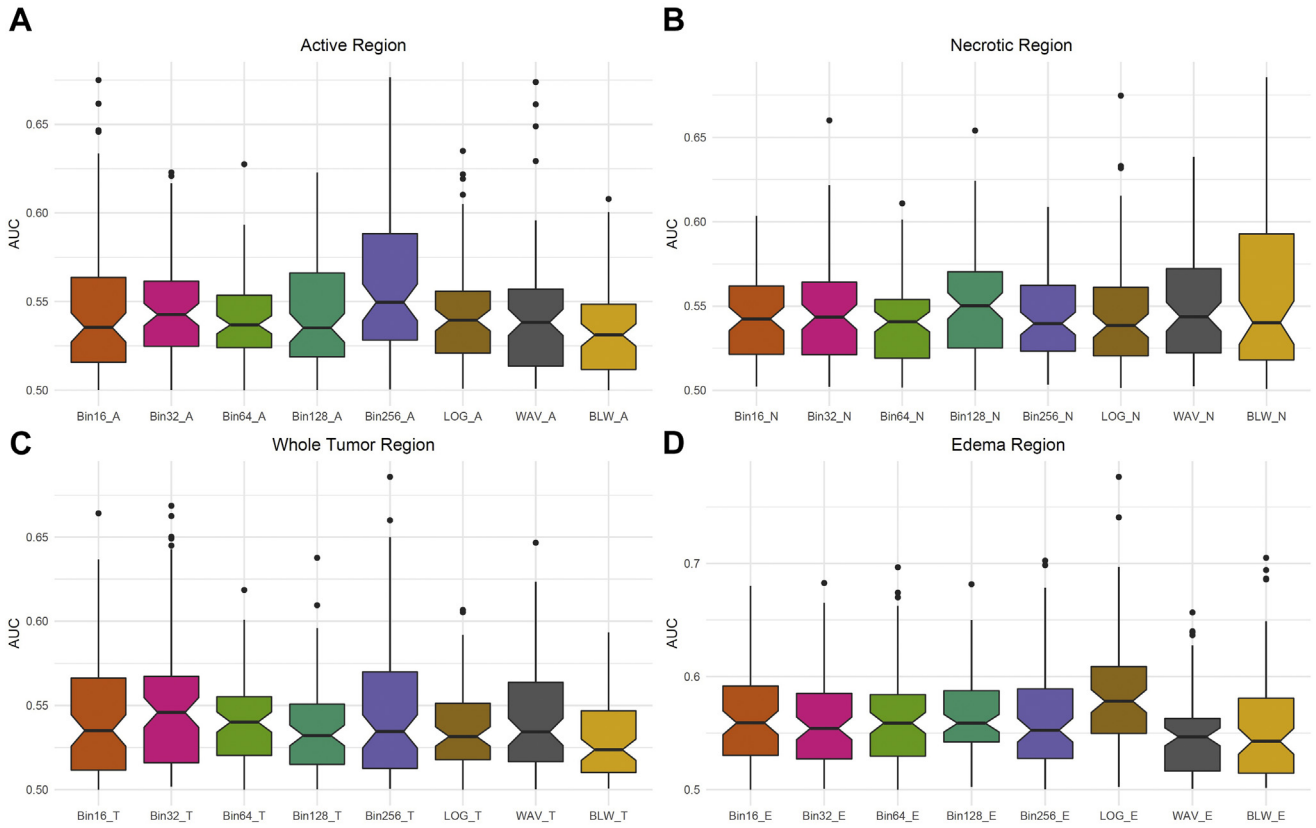

Figure 4. (**A**) Boxplot showing predictive performance (area under the curve [AUC]) (y axis) of active tumor region image sets (x axis). (**B**) Boxplot showing predictive performance (AUC) (y axis) of necrosis tumor region image sets (x axis). (**C**) Boxplot showing predictive performance (AUC) (y axis) of whole tumor region image sets (x axis). (**D**) Boxplot showing predictive performance (AUC) (y axis) of edema tumor region image sets (x axis).

Machine (SVM) and Random Forest (RF) classifier on GLCM and Gray Level Run Length Matrix features extracted from T1-W-CE and T2-W images ineEnhanced region. Their results showed that the RF classifier had AUC, 0.75 from T1-W-CE and AUC, 0.84 from T2-W. The SVM classifier had an AUC, 0.76 from T1-W-CE and AUC, 0.85 from T2-W. This developed model was found to be a high-performance predictive model. Performance of our model in the enhanced region is lower than that found in this study (**Supplementary Figure 1**). However, Korfiatis et al. did not extract features from other regions, and the extracted features were limited. Our results show that SVM classifier in combination with all features (BWL image set) in the necrotic region had the best performance (AUC, 0.68).

Xi et al.[22] reported that combinations of sequences improved prediction performance as opposed to singular sequences. These investigators found that T1-W imaging, T2-W imaging, and enhanced T1-W imaging radiomics features could predict MGMT promoter methylation with an accuracy of 86.59% in the training cohort and 80% in the validation cohort. This study extracted features from WTs, used SVM for classification, and LASSO for feature selection. Our results show that Bin 64 and LOG filter + shape features with combinations of 4 segments in T1-W-CE and FLAIR has the best performance.

Furthermore, Wei et al.[35] reported that ADC values are correlated with MGMT methylation status. However, these investigators also found that T1-W CE and T2 FLAIR sequences had better performances than ADC. Regarding the diffusion-weighted imaging, the extracted ADC value was found to be a predictor for MGMT promoter methylation status, with a sensitivity of 84% and a specificity of 91%. The fusion radiomics signature model had the best performance. Our model performed well in the necrotic region when combining Bin, LOG, and wavelet (BLW) filters.

In this study, multiregional segmentation was used for feature extraction in 2 magnetic resonance sequences (**Figure 1**). Regions were also combined to investigate which have more prediction power (**Figure 5A**). In addition, the impact of MRI preprocessing and combining regions with differing MLs on the prediction of tumor MGMT mutation status was evaluated. However, this field lacks a comprehensive guideline for the optimal usage of robots features[36,37] and classifiers.[11] Therefore, this study attempted to determine the best classifier

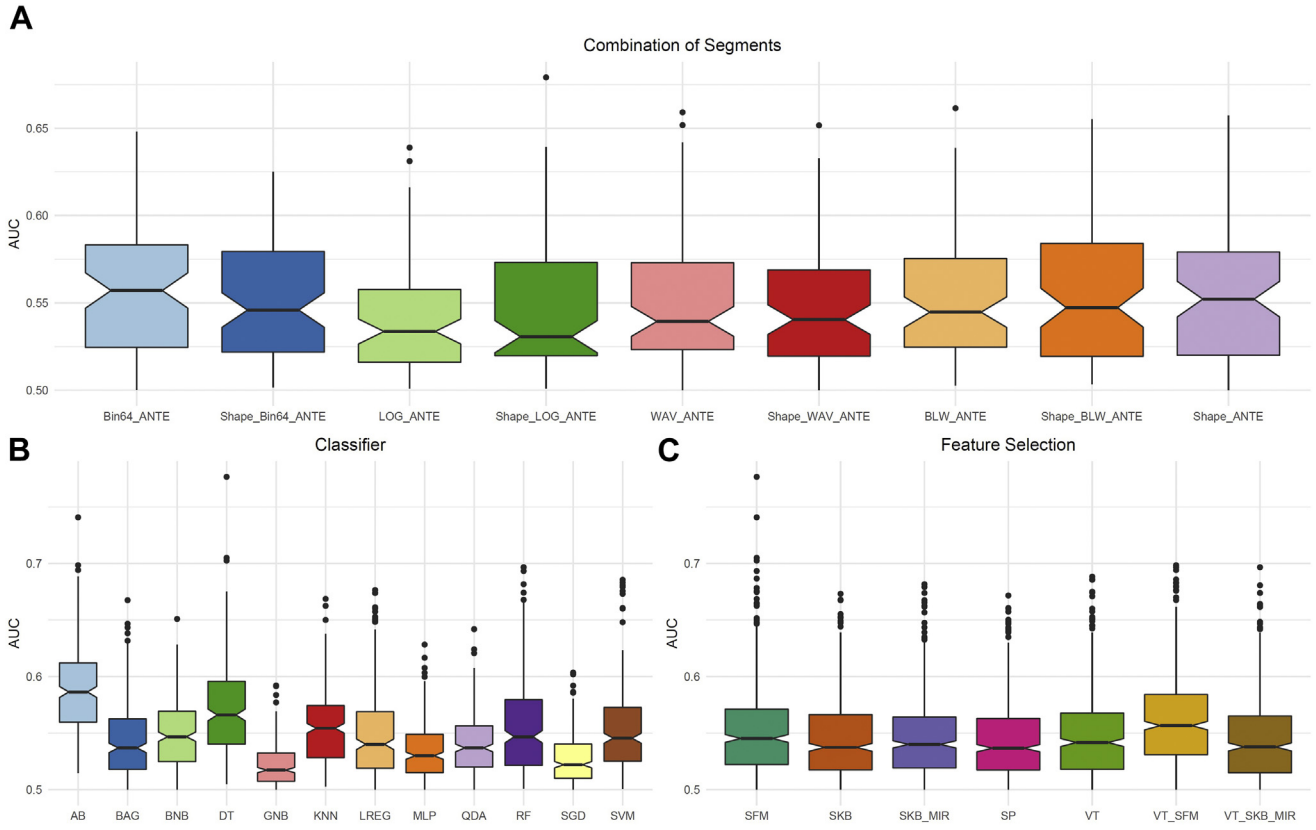

Figure 5. (**A**) Boxplot show predictive performance (area under the curve [AUC]) (y axis) of combination of all tumor regions image sets (x axis). (**B**) Boxplot show predictive performance (AUC) (y axis) of feature selection methods (x axis). (**C**) Boxplot show predictive performance (AUC) (y axis) of classifier methods (x axis).

and feature selector for such investigations. The impact of preprocessing MRIs on MGMT methylation status determination was evaluated. The main limitation of this study was the size of the data set. To overcome this limitation, models were validated using 10-fold cross-validation to reduce the sensitivity of the results to input data, as well as to increase reliability. Future studies should use larger data sets that contain external validation sets.

CONCLUSIONS

This study showed that radiomics using ML algorithms is a feasible noninvasive approach to predict MGMT methylation status in patients with GBM cancer. Also, some radiomics could predict the issue alone or in combination with other features. This factor is important because it could narrow down the treatment options for patients and increase the safety and efficacy of the procedures.

REFERENCES

1. Ostrom QT, Gittleman H, Farah P, et al. CBTRUS statistical report: Primary brain and central nervous system tumors diagnosed in the United States in 2006-2010. *Neuro Oncol*. 2013;15(suppl 2): ii1-ii56.
2. Stupp R, Hegi ME, Mason WP, et al. Effects of radiotherapy with concomitant and adjuvant temozolomide versus radiotherapy alone on survival in glioblastoma in a randomised phase III study: 5-year analysis of the EORTC-NCIC trial. *Lancet Oncol*. 2009;10:459-466.
3. Reardon DA, Wen PY. Glioma in 2014: Unravelling tumour heterogeneity—implications for therapy. *Nature Rev Clin Oncol*. 2015;12:69.
4. Wick W, Hartmann C, Engel C, et al. NOA-04 randomized phase III trial of sequential radiochemotherapy of anaplastic glioma with procarbazine, lomustine, and vincristine or temozolomide. *J Clin Oncol*. 2009;27:5874.
5. Hegi ME, Diserens A-C, Gorlia T, et al. MGMT gene silencing and benefit from temozolomide in glioblastoma. *N Engl J Med*. 2005;352:997-1003.
6. Donson AM, Addo-Yobo SO, Handler MH, Gore L, Foreman NK. MGMT promoter methylation correlates with survival benefit and sensitivity to temozolomide in pediatric glioblastoma. *Pediatr Blood Cancer*. 2007;48:403-407.
7. Dunn J, Baborie A, Alam F, et al. Extent of MGMT promoter methylation correlates with outcome in glioblastomas given temozolomide and radiotherapy. *Br J Cancer*. 2009;101:124-131.
8. Rivera AL, Pelloski CE, Gilbert MR, et al. MGMT promoter methylation is predictive of response to radiotherapy and prognostic in the absence of

adjuvant alkylating chemotherapy for glioblastoma. *Neuro Oncol*. 2010;12:116-121.

9. Ellingson BM, Wen PY, van den Bent MJ, Cloughesy TF. Pros and cons of current brain tumor imaging. *Neuro Oncol*. 2014;16(suppl 7): vii2-viii1.

10. Hu LS, Ning S, Eschbacher JM, et al. Multi-parametric MRI and texture analysis to visualize spatial histologic heterogeneity and tumor extent in glioblastoma. *PLoS One*. 2015;10:e0141506.

11. Abdollahi H, Mofid B, Shiri I, et al. Machine learning-based radiomic models to predict intensity-modulated radiation therapy response, Gleason score and stage in prostate cancer. *Radiol Med*. 2019b;124:555-567.

12. Abdollahi H, Mostafaei S, Cheraghi S, Shiri I, Mahdavi SR, Kazemnejad A. Cochlea CT radiomics predicts chemoradiotherapy induced sensorineural hearing loss in head and neck cancer patients: a machine learning and multi-variable modelling study. *Phys Med*. 2018;45:192-197.

13. Lambin P, Rios-Velazquez E, Leijenaar R, et al. Radiomics: extracting more information from medical images using advanced feature analysis. *Eur J Cancer*. 2012;48:441-446.

14. Narang S, Lehrer M, Yang D, Lee J, Rao A. Radiomics in glioblastoma: current status, challenges and potential opportunities. *Translational Cancer Research*. 2016;5:383-397.

15. Abdollahi H, Mahdavi SR, Shiri I, Mofid B, Bakhshandeh M, Rahmani K. Magnetic resonance imaging radiomic feature analysis of radiation-induced femoral head changes in prostate cancer radiotherapy. *J Cancer Res Ther*. 2019a;15:11.

16. Abdollahi H, Shiri I, Heydari M. Medical imaging technologists in radiomics era: an Alice in Wonderland problem. *Iran J Public Health*. 2019c; 48:184.

17. Aerts HJ, Velazquez ER, Leijenaar RT, et al. Decoding tumour phenotype by noninvasive imaging using a quantitative radiomics approach. *Nat Commun*. 2014;5:4006.

18. Ellingson BM. Radiogenomics and imaging phenotypes in glioblastoma: novel observations and correlation with molecular characteristics. *Curr Neurol Neurosci Rep*. 2015;15:506.

19. Prayson RA, Agamanolis DP, Cohen ML, et al. Interobserver reproducibility among neuropathologists and surgical pathologists in fibrillary astrocytoma grading. *J Neurol Sci*. 2000;175:33-39.

20. Sanai N, Martino J, Berger MS. Morbidity profile following aggressive resection of parietal lobe gliomas: clinical article. *J Neurosurg*. 2012;116: 1182-1186.

21. Moon W-J, Choi JW, Roh HG, Lim SD, Koh Y-C. Imaging parameters of high grade gliomas in relation to the MGMT promoter methylation status: the CT, diffusion tensor imaging, and perfusion MR imaging. *Neuroradiology*. 2012;54:555-563.

22. Xi Y-B, Guo F, Xu Z-L, et al. Radiomics signature: a potential biomarker for the prediction of MGMT promoter methylation in glioblastoma: GBM radiomics features reflect MGMT. *J Magn Reson Imaging*. 2018;4:1380-1387.

23. Korfiatis P, Kline TL, Coufalova L, et al. MRI texture features as biomarkers to predict MGMT methylation status in glioblastomas. *Med Phys*. 2016;43:10.

24. Iliadis G, Kotoula V, Chatzisotiriou A, et al. Volumetric and MGMT parameters in glioblastoma patients: survival analysis. *BMC Cancer*. 2012; 12:3.

25. Levner I, Drabycz S, Roldan G, De Robles P, Cairncross JG, Mitchell R. Predicting MGMT methylation status of glioblastomas from MRI texture. In: Yang G-Z, Hawkes D, Rueckert D, Noble A, Taylor C, eds. *Lecture Notes in Computer Science*. Berlin, Heidelberg: Springer; 2009:522-530.

26. Eoli M, Menghi F, Bruzzone MG, et al. Methylation of O6-methylguanine DNA methyltransferase and loss of heterozygosity on 19q and/or 17p are overlapping features of secondary glioblastomas with prolonged survival. *Clin Cancer Res*. 2007;13:2606-2613.

27. Drabycz S, Roldán G, de Robles P, et al. An analysis of image texture, tumor location, and MGMT promoter methylation in glioblastoma using magnetic resonance imaging. *Neuroimage*. 2010;49:1398-1405.

28. Clark K, Vendt B, Smith K, et al. The Cancer Imaging Archive (TCIA): maintaining and operating a public information repository. *J Digital Imaging*. 2013;26:1045-1057.

29. The Cancer Imaging Archive. Available at: http://cancerimagingarchive.net. Accessed 25 September 2017.

30. The Cancer Genome Atlas. Available at: https://cancergenome.nih.gov/. Accessed 25 September 2017.

31. Bady P, Sciuscio D, Diserens A-C, et al. MGMT methylation analysis of glioblastoma on the Infinium methylation BeadChip identifies two distinct CpG regions associated with gene silencing and outcome, yielding a prediction model for comparisons across datasets, tumor grades, and CIMP-status. *Acta Neuropathol*. 2012; 124:547.

32. Li Z-C, Bai H, Sun Q, et al. Multiregional radiomics features from multiparametric MRI for prediction of MGMT methylation status in glioblastoma multiforme: a multicentre study. *Eur Radiol*. 2018;28:3640-3650.

33. Diehn M, Nardini C, Wang, et al. Identification of noninvasive imaging surrogates for brain tumor gene-expression modules. *Proc Natl Acad Sci U S A*. 2008;105:5213-5218.

34. Kanas VG, Zacharaki EI, Thomas GA, Zinn PO, Megalooikonomou V, Colen RR. Learning MRI-based classification models for MGMT methylation status prediction in glioblastoma. *Comput Methods Programs Biomed*. 2017;140:249-257.

35. Wei J, Yang G, Hao X, et al. A multi-sequence and habitat-based MRI radiomics signature for preoperative prediction of MGMT promoter methylation in astrocytomas with prognostic implication. *Eur Radiol*. 2019;29:877-888.

36. Shiri I, Abdollahi H, Shaysteh S, Mahdavi SR. Test-retest reproducibility and robustness analysis of recurrent glioblastoma MRI radiomics texture features. *Iran J Radiol*. 2017a;5. https://doi.org/10.5812/iranjradiol.48035.

37. Shiri I, Rahmim A, Ghaffarian P, Geramifar P, Abdollahi H, Bitarafan-Rajabi A. The impact of image reconstruction settings on 18F-FDG PET radiomic features: multi-scanner phantom and patient studies. *Eur Radiol*. 2017b;27:4498-4509.

Conflict of interest statement: This study was funded by Rajaie Cardiovascular Medical and Research Center, Iran University of Medical Science and Kermanshah University of Medical Sciences, Iran (grant number 980002).

Received 15 July 2019; accepted 29 August 2019

Citation: World Neurosurg. (2019) 132:e140-e161. https://doi.org/10.1016/j.wneu.2019.08.232

*Journal homepage: **www.journals.elsevier.com/world-neurosurgery***

*Available online: **www.sciencedirect.com***

1878-8750/$ - see front matter

SUPPLEMENTARY DATA

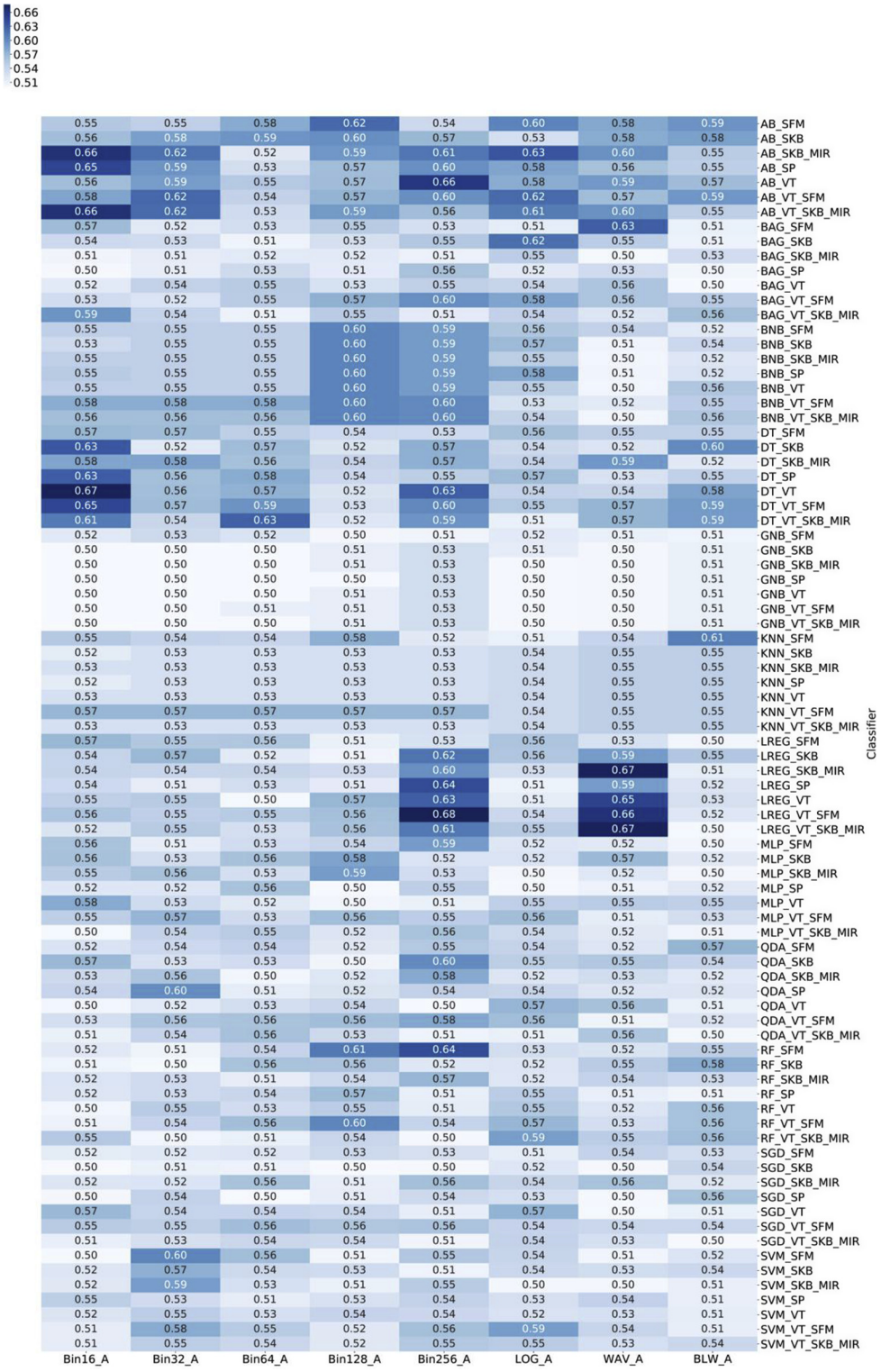

Supplementary Figure 1. Heatmap depicting the predictive performance (area under the curve) of feature selection/classification methods (*rows*) and active tumor region image sets (*columns*) in prediction MGMT methylation status.

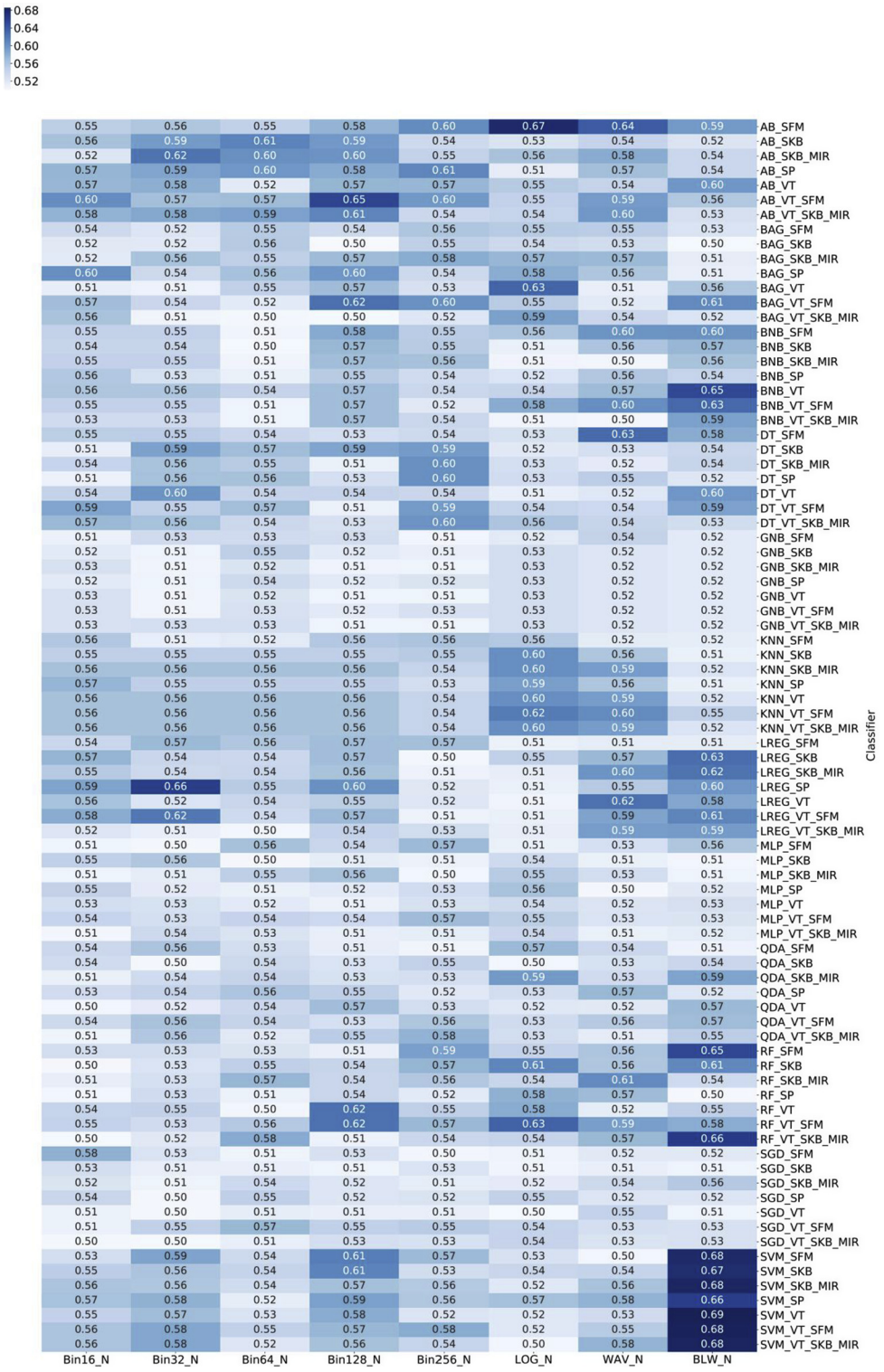

Supplementary Figure 2. Heatmap depicting the predictive performance (area under the curve) of feature selection/classification methods (*rows*) and necrosis tumor region image sets (*columns*) in prediction MGMT methylation status.

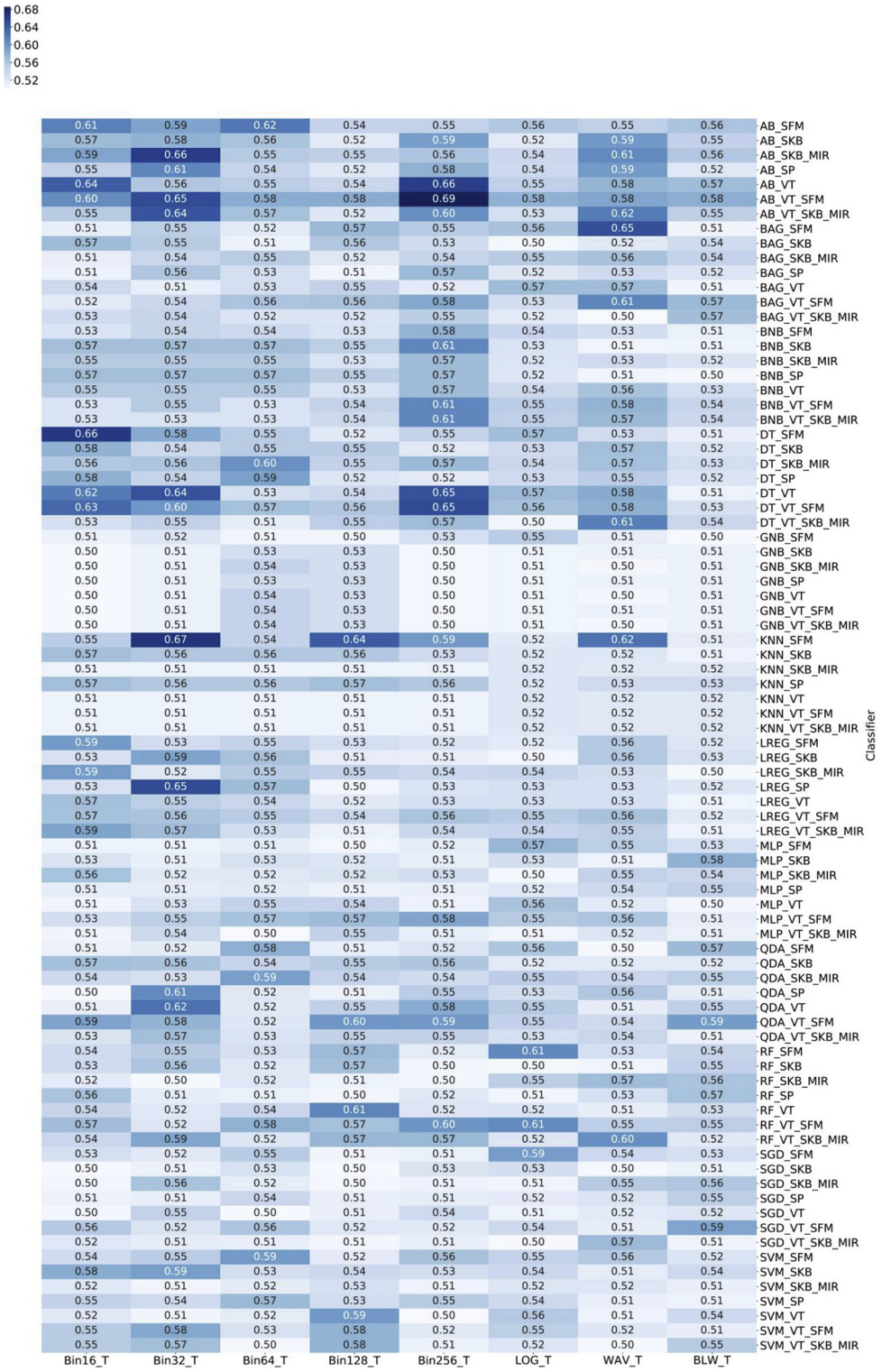

Supplementary Figure 3. Heatmap depicting the predictive performance (area under the curve) of feature selection/classification methods (*rows*) and whole tumor region image sets (*columns*) in prediction MGMT methylation status.

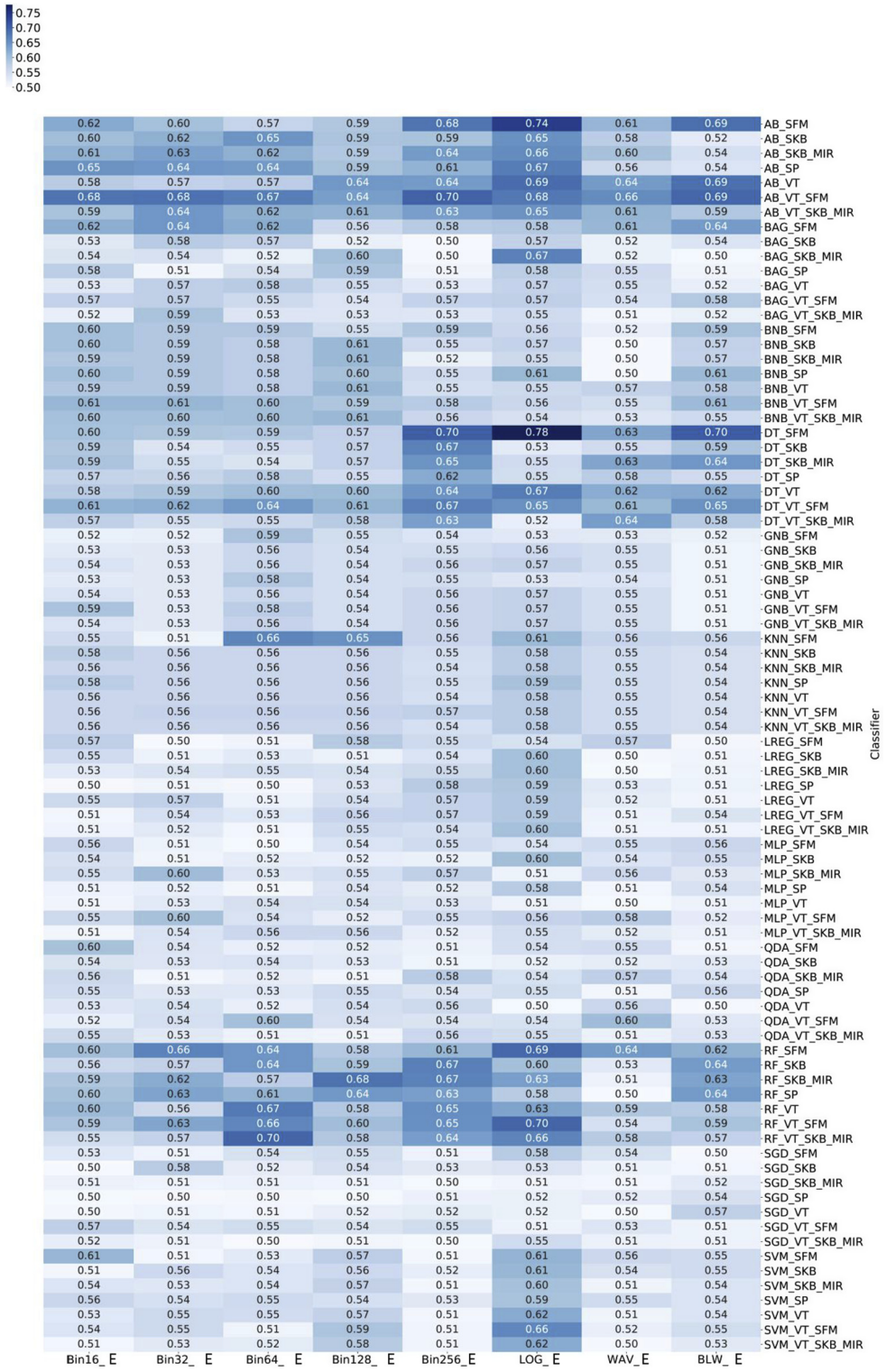

Supplementary Figure 4. Heatmap depicting the predictive performance (area under the curve) of feature selection/classification methods (*rows*) and edema region image sets (*columns*) in prediction MGMT methylation status.

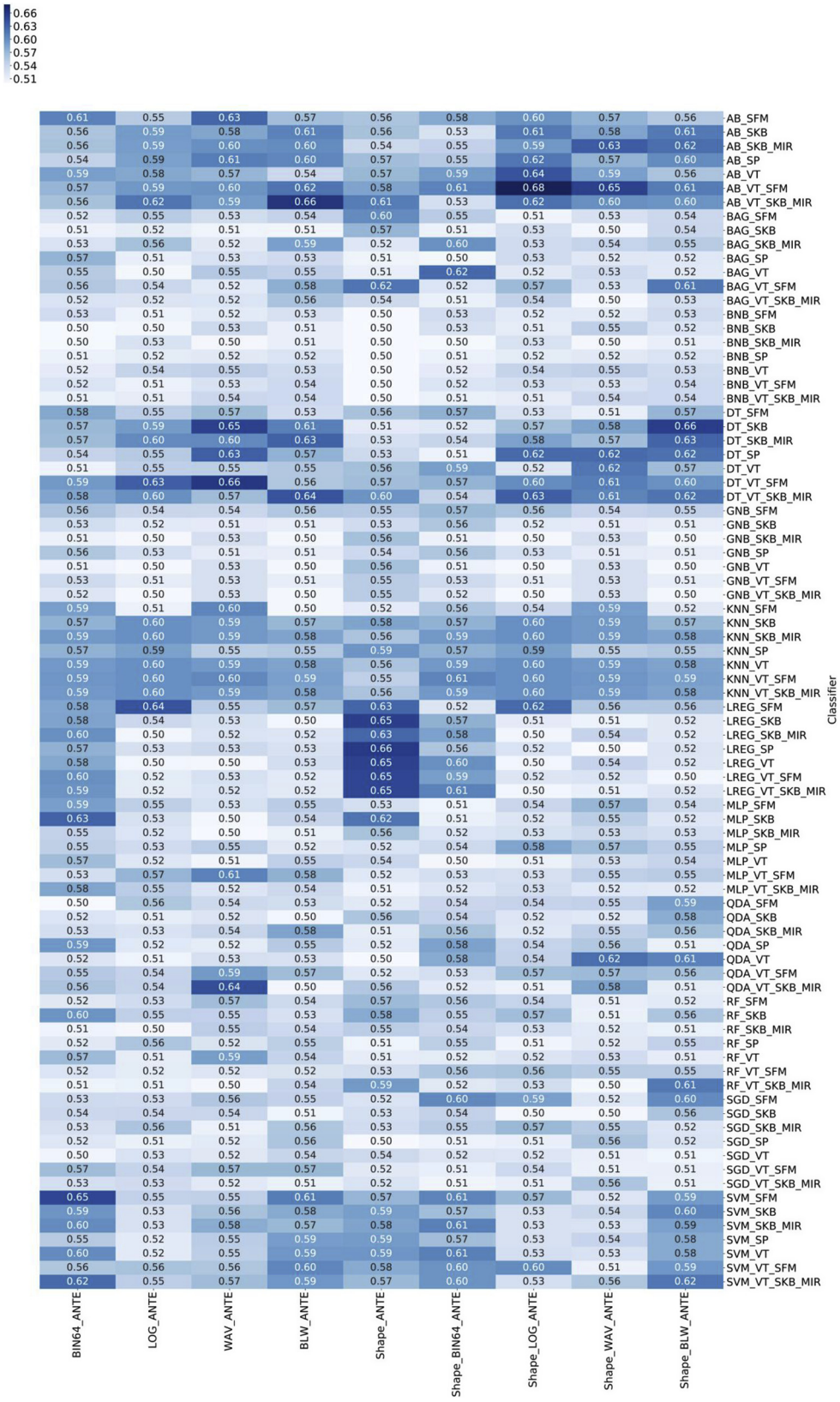

Supplementary Figure 5. Heatmap depicting the predictive performance (area under the curve) of feature selection/classification methods (*rows*) and combination of all tumor regions image sets (*columns*) in prediction MGMT methylation status.

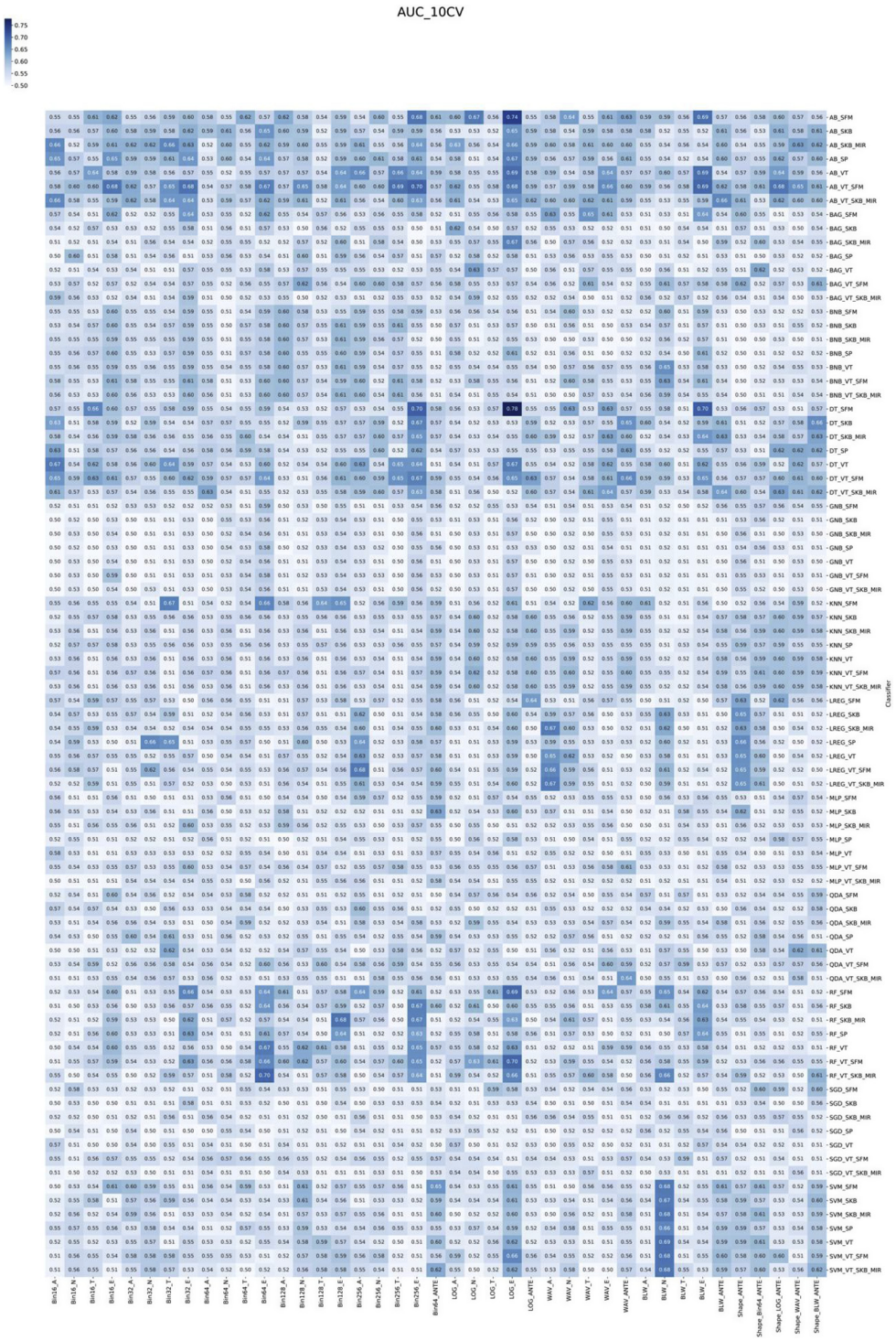

Supplementary Figure 6. Heatmap depicting the predictive performance (area under the curve) of feature selection/classification methods (*rows*) and image sets (*columns*) in prediction MGMT methylation status.

Supplementary Table 1. Radiomics Features

First Order Statistics (FOS)	Gray Level Co-occurrence Matrix	Gray Level Run Length Matrix (GLRLM)	Shape features	Gray Level Size Zone Matrix (GLSZM)	Gray Level Dependence Matrix (GLDM)	Neighboring Gray Tone Difference Matrix (NGTDM)
Energy	Autocorrelation	Short Run Emphasis (SRE)	Volume	Small Area Emphasis (SAE)	Small Dependence Emphasis (SDE)	Coarseness
Total energy	Joint Average	Long Run Emphasis (LRE)	Surface area	Large Area Emphasis (LAE)	Large Dependence Emphasis (LDE)	Contrast
Entropy	Cluster Prominence	Gray Level Non-Uniformity (GLN)	Surface area to volume ratio	Gray Level Non-Uniformity (GLN)	Gray Level Non-Uniformity (GLN)	Busyness
Minimum	Cluster Shade	Gray Level Non-Uniformity Normalized (GLNN)	Sphericity	Gray Level Non-Uniformity Normalized (GLNN)	Dependence Non-Uniformity (DN)	Complexity
10th percentile	Cluster Tendency	Run Length Non-Uniformity (RLN)	Compactness 1	Size Zone Non-Uniformity (SZN)	Dependence Non-Uniformity Normalized (DNN)	Strength
90th percentile	Contrast	Run Length Non-Uniformity Normalized (RLNN)	Compactness 2	Size Zone Non-Uniformity Normalized (SZNN)	Gray Level Variance (GLV)	
Maximum	Correlation	Run Percentage (RP)	Spherical disproportion	Zone Percentage (ZP)	Dependence Variance (DV)	
Mean	Difference Average	Gray Level Variance (GLV)	Maximum 3D diameter	Gray Level Variance (GLV)	Dependence Entropy (DE)	
Median	Difference Entropy	Run Variance (RV)	Maximum 2D diameter (slice)	Zone Variance (ZV)	Low Gray Level Emphasis (LGLE)	
Interquartile range	Difference Variance	Run Entropy (RE)	Maximum 2D diameter (column)	Zone Entropy (ZE)	High Gray Level Emphasis (HGLE)	
Range	Joint Energy	Low Gray Level Run Emphasis (LGLRE)	Maximum 2D diameter (row)	Low Gray Level Zone Emphasis (LGLZE)	Small Dependence Low Gray Level Emphasis (SDLGLE)	
Mean absolute deviation (MAD)	Joint Entropy	High Gray Level Run Emphasis (HGLRE)	Major axis	High Gray Level Zone Emphasis (HGLZE)	Small Dependence High Gray Level Emphasis (SDHGLE)	
Robust mean absolute deviation (rMAD)	Informal Measure of Correlation (IMC) 1	Short Run Low Gray Level Emphasis (SRLGLE)	Minor axis	Small Area Low Gray Level Emphasis (SALGLE)	Large Dependence Low Gray Level Emphasis (LDLGLE)	
Root mean squared (RMS)	Informal Measure of Correlation (IMC) 2	Short Run High Gray Level Emphasis (SRHGLE)	Least axis	Small Area High Gray Level Emphasis (SAHGLE)	Large Dependence High Gray Level Emphasis (LDHGLE)	
Standard deviation	Inverse Difference Moment (IDM)	Long Run Low Gray Level Emphasis (LRLGLE)	Elongation	Large Area Low Gray Level Emphasis (LALGLE)		
Skewness	Inverse Difference Moment Normalized (IDMN)	Long Run High Gray Level Emphasis (LRHGLE)	Flatness	Large Area High Gray Level Emphasis (LAHGLE)		
Kurtosis	Inverse Difference (ID)		A/T volume ratio			

Variance	Inverse Difference Normalized (IDN)		N/T volume ratio			
Uniformity	Inverse Variance		T/E volume ratio			
	Maximum Probability					
	Sum Average					
	Sum Entropy					
	Sum of Squares					

Supplementary Table 2. Image Datasets

Filter	Segment	Number of Features	Number of Image Sets
SHAPE	ANTE	55	1
BIN 16	A, N, T, E	92	4
BIN 32	A, N, T, E	92	4
BIN 64	A, N, T, E, ANTE SHAPE + ANTE	92 368 423	4 1 1
BIN 128	A, N, T, E	92	4
BIN 256	A, N, T, E	92	4
LOG	A, N, T, E, ANTE SHAPE + ANTE	920 3680 3735	4 1 1
WAV	A, N, T, E, ANTE SHAPE + ANTE	736 2944 2999	4 1 1
BIN 64+LOG+WAV	A, N, T, E, ANTE SHAPE + ANTE	1748 6992 7047	4 1 1
SUM		8519	41

Supplementary Table 3. Classifier Parameters Detail

Classification Methods	Classification Methods
Adaptive Boost[1]	Base Estimator: Decision Tree Classifier Number estimators (number of estimators at which boosting is terminated): 50 Learning rate:1 Algorithm: {'SAMME.R'} Random state: random state instance (random state is the random number generator)
Bagging[2]	Base Estimator: Decision Tree N estimators (number of base estimators): 20 Max samples (number of samples to draw from X to train each base estimator): 10 Max features (number of features to draw from X to train each base estimator): 20 Bootstrap: true Bootstrap features: false OOB score (out-of-bag samples to estimate the generalization error): false Random state: random state instance (random state is the random number generator)
Decision Tree[3]	Criterion (the function to measure the quality of a split): GINI Splitter: best Max depth: nodes are expanded until all leaves are pure Min samples split: 2 Min samples leaf: 1 Min weight fraction leaf: 0.0 Max features: consider max features at each split Random state: true Max leaf nodes: unlimited number of leaf nodes Min impurity decrease: 0.0 Class weight: one for each class Presort: false
Gaussian Naive Bayes[4]	Priors (prior probability of each class): according to data distribution
K-Nearest Neighbors[5]	N neighbors: 5 Weights: distance Algorithm: 'auto' Leaf size: 30 P (power parameter for the Minkowski metric): Minkowski distance Metric: 'minkowski'
Logistic Regression[6]	Penalty: L2 TOL (tolerance for stopping criteria): 1e−4 C (inverse of regularization strength): 1 Fit intercept: true Intercept scaling (the synthetic feature weight is subject to l1/l2 regularization as all other features): 1 Class weight: balanced Random state: random state instance (random state is the random number generator) Solver: 'liblinear' Max iter: 100 Warm start (fit a whole new ensemble): false

Continues

Supplementary Table 3. Continued

Classification Methods	Classification Methods
Multilayer Perceptron[7]	Hidden layer sizes: (100,) activation: tanh solver (solver for weight optimization.): Adam alpha (L2 penalty "regularization term" parameter): 0.0001 Batch size: number of samples Learning rate: adaptive Learning rate init: 0.001 Max iterations (maximum number of iterations): 1000 Shuffle: true Momentum: 0.9 TOL (tolerance for stopping criteria): 1e-4 Beta 1 (exponential decay rate for estimates of first moment vector in Adam): 0.9 Beta 2 (exponential decay rate for estimates of second moment vector in Adam): 0.999 Epsilon: 1e−8
Quadratic Discriminant Analysis[8]	Priors (prior probability of each class): according to data distribution Store covariance: true TOL (tolerance for stopping criteria): 1e−4
Random Forest[9]	N estimators (number of estimators): 50 Criterion: MSE Max depth: expanded until all leaves are pure Min samples leaf (minimum number of samples required to be at a leaf node): 1 Min weight fraction leaf: 0.0 Max features: 'auto' Max leaf nodes: none Min impurity split (threshold for early stopping in tree grow): none Min impurity decrease: 0.0 Bootstrap: true OOB score: (out-of-bag samples to estimate the generalization error): false
Stochastic Gradient Descent[10]	Loss: hinge Penalty: 'l2' Alpha: 0.0001 Fit intercept: true TOL (tolerance for stopping criteria): 1e−4 Shuffle: true Random state: random state instance (random state is the random number generator) Learning rate: 'optimal' (1.0/(alpha × (t + t0))) Power t: 0.5 Class weight: balanced
Naive Bayesian[11]	Priors (prior probability of each class): according to data distribution
Support Vector Machine[12]	C: 1.0 Kernel: RBF Degree: 3 Gamma: 1/number features Shrinking: use the shrinking heuristic Probability: false TOL (tolerance for stopping criteria): 1e−4 Class weight: balanced Max iteration: no limit Decision function shape: one-vs-rest Random state: random state instance (random state is the random number generator)

REFERENCES

1. Hastie T, Rosset S, Zhu J, Zou H. Multi-class adaboost. *Statistics and its Interface*. 2009;2:349-360.
2. Breiman L. Bagging predictors. *Machine Learning*. 1996;24:123-140.
3. Quinlan JR. Induction of decision trees. *Machine Learning*. 1986;1:81-106.
4. Zhang H. The optimality of naive Bayes. AA. 2004;1:3.
5. Cunningham P, Delany SJ. k-Nearest neighbour classifiers. *Multiple Classifier Systems*. 2007;34:1-17.
6. Fan R-E, Chang K-W, Hsieh C-J, Wang X-R, Lin C-J. LIBLINEAR: A library for large linear classification. *Journal Machine Learning Research*. 2008;9:1871-1874.
7. Haykin SS, Haykin SS, Haykin SS, Haykin SS. *Neural Networks and Learning Machines*. Upper Saddle River, NJ: Pearson; 2009.
8. Srivastava S, Gupta MR, Frigyik BA. Bayesian quadratic discriminant analysis. *Journal Machine Learning Research*. 2007;8:1277-1305.
9. Breiman L. Random forests. *Machine Learning*. 2001;45:5-32.
10. Tsuruoka Y, Tsujii JI, Ananiadou S, eds. *Stochastic gradient descent training for l1-regularized log-linear models with cumulative penalty. Proceedings of the Joint Conference of the 47th Annual Meeting of the ACL and the 4th International Joint Conference on Natural Language Processing of the AFNLP: Volume 1*. Suntec, Singapore: Association for Computational Linguistics; 2009.
11. Rish I, ed. *An Empirical Study of the Naive Bayes Classifier. IJCAI 2001 Workshop on Empirical Methods in Artificial Intelligence*. New York, NY: IBM; 2001.
12. Suykens JA, Vandewalle J. Least squares support vector machine classifiers. *Neural Processing Lett*. 1999;9:293-300.